

An *ab initio* study of adsorption of alanine on the chiral calcite(21 $\bar{3}$ 1) surface

A. ASTHAGIRI^{†‡*} and R. M. HAZEN[†]

[†]Geophysical Laboratory, Carnegie Institution of Washington, Washington, DC 20015 USA

[‡]Department of Chemical Engineering, University of Florida, Gainesville, FL 32611, USA

(Received June 2006; revised September 2006)

Density functional theory calculations has been used to examine the adsorption of D- and L-alanine (Ala) on the chiral calcite(21 $\bar{3}$ 1) surface. We find negligible differences (< 1 kcal/mol) in adsorption energies for the most stable minima of D- and L-Ala on the calcite(21 $\bar{3}$ 1) surface. The strongest interaction in the adsorbed system is between the surface Ca and the O atom of the carboxyl group on Ala. The source of the weak enantiospecificity is the relative difference in dimensions of the Ala and the atoms on the calcite(21 $\bar{3}$ 1) surface. The surface O and Ca atoms on the calcite(21 $\bar{3}$ 1) surface are separated by 6 Å, while the Ala molecule is roughly 3–4 Å in size. This disparity in dimensions prevents the Ala molecule from making three strong points of contact with the surface, a prerequisite for strong enantiospecificity.

Keywords: Chirality; Density functional theory; Mineral surfaces; Calcite; Amino acid

1. Introduction

The source of life's homochirality remains one of the most profound questions in origin-of-life research. Chiral mineral surfaces have been postulated as a plausible source of symmetry breaking at the very early stages of life on earth [1–3]. Recently, Hazen and co-workers have demonstrated experimentally that chiral faces of the mineral calcite (CaCO₃) can discriminate between enantiomers of amino acids [2]. In particular, they found L-aspartic acid (Asp) adsorbs preferentially versus D-Asp on the (3 $\bar{1}$ 21) face (in the hexagonal morphological setting [4]), while the inverse was found on the mirror (21 $\bar{3}$ 1) face. This result has implications for the origins of life's homochirality, if one conjectures that particular chiral faces of minerals, such as calcite, might have imposed a local chiral preference in the early stages of peptide formation [1,2]. Despite the experimental work of Hazen *et al.*, an understanding of the atomic level interactions at the amino acid–chiral mineral interface is still needed. In this paper we examine the enantiospecific adsorption of Ala, the simplest chiral amino acid, on CaCO₃(21 $\bar{3}$ 1) using density functional theory (DFT). While DFT cannot directly simulate the complex experimental system, it allows us to link quantitative measures of enantiospecificity

with specific mineral–amino acid interactions that are the source of the enantiospecificity.

In the last several years, there has been considerable interest in the enantiospecific behavior of naturally chiral surfaces for its potential use, in enantioselective synthesis of chiral pharmaceuticals (see Ref. [5] and references therein). Much of this work has concentrated on naturally chiral metal surfaces, which can be obtained by exposing high Miller surfaces [6,7]. Adsorption of chiral organic molecules on various chiral metal surfaces [6,8–12] has been examined both experimentally and theoretically. Temperature programmed desorption studies of various chiral molecules on the chiral Cu(643) surface have detected enantiospecific binding energies varying from 0.25 to 0.06 kcal/mol [7,12–14]. Similar enantiospecific binding energies have been found in theoretical studies of physisorption of cyclic chiral hydrocarbons on chiral Pt surfaces [6,8–10,15]. Sljivancanin *et al.* have examined the chemisorption of a chiral molecule, (S)- and (R)-HSCH₂CHNH₂CH₂P(CH₃)₂, on the chiral Au(17 11 9) surface using DFT [16]. Such chemisorbed systems should have a stronger interaction than physisorbed systems and one may expect a correspondingly larger enantiospecific effect. In fact, Sljivancanin *et al.* found that the S-enantiomer adsorbed 2.1 kcal/mol more strongly than the

*Corresponding author. Email: aasthagiri@che.ufl.edu

R-enantiomer. Furthermore, they found that to obtain an enantiospecific effect required three strong points of interaction with the chiral surface, and in their molecule these interactions are due to the thiol, amino, and phosphino groups. Molecules with one of these interactions removed did not show significant enantiospecificity. Recently, Bhatia and Sholl examined enantiospecific adsorption of amino-(fluoro)methoxy (FAM) and propylene oxide (PO) on the Cu(874) surface using DFT [17]. They found that FAM shows an enantiospecific binding of 3.0 kcal/mol, while PO shows a small 0.46 kcal/mol difference. PO interacts with the Cu link through two hydrogen atoms and one oxygen atom, which allows for very similar interactions to occur between the enantiomers of PO. For FAM one of the hydrogen-Cu surface interactions is replaced by a F-Cu surface interaction, which allow for a much more restrictive geometry for the adsorbate. These findings are again consistent with the view that strong enantiospecific adsorption will be found when three strong interactions occur with the surface. Amino acids adsorbed on achiral metal surfaces have also been studied by various groups (see Ref. [18] and references therein) and DFT has been used to clarify some confusion on the exact configuration taken by the amino acids on the metal surfaces [19,20].

While the work on chiral metal surfaces has firmly established the ability of naturally chiral surfaces in differentiating enantiomers of a wide range of chiral molecules, there has been considerably less work done on chiral mineral surfaces. As noted earlier, chiral mineral surfaces may have provided the local environment for symmetry breaking that led to homochiral life on earth. Furthermore, a vast array of chiral mineral and metal oxide surfaces are available for industrial applications [4–6,21] surfaces that are substantially cheaper and more diverse chemically than metal surfaces. Most early work focused on adsorption of chiral molecules on quartz (SiO_2), the only common chiral mineral, but these studies were on polycrystalline samples rather than on a particular chiral face [22,23]. Insight on the interaction of chiral molecules and minerals is also provided by extensive work on the effect of calcite dissolution in the presence of a chiral amino acid solution. Teng *et al.* observed the appearance of chiral growth features and etch pits on the achiral calcite($10\bar{1}1$) in the presence of L-Asp solution and a mirror image in the presence of D-Asp [24–26]. Semiempirical calculations of the adsorption of D- and L-Asp on the acute and obtuse steps found on calcite($10\bar{1}1$) demonstrated that the enantiospecific binding at the steps of calcite($10\bar{1}1$) surface is the source of the enantiospecific morphological features observed [26]. These modeling results match the observations of the chiral morphology of growth hillocks obtained from *in situ* atomic force microscopy of calcite growth in the presence of enantiomeric Asp solution.

Hazen and co-workers examined the adsorption of Asp on the six faces of the $\{12\bar{3}1\}$ chiral trigonal scalenohedral calcite surface [2]. Each of the six faces can be identified

as an R or L surface and related to each other by a mirror. Crystals having all six faces were immersed in a racemic solution of Asp, the adsorbed material was then removed with an acid wash and the D/L ratios were determined using gas chromatography. They found $D/L > 1$ on the R surfaces and $D/L < 1$ on the L surfaces. This result indicates that D-Asp binds more strongly on the R faces of this surface. One of the R faces is $\text{CaCO}_3(21\bar{3}1)$, which is the chiral surface that is the focus of our study. Recently, Downs and Hazen have proposed a chiral index to measure the enantioselective potential of chiral surfaces based on atomic displacements from ideal mirror or glide plane symmetry [27]. Applying the chiral index to various chiral metal and mineral surfaces, Downs and Hazen found that the $\text{CaCO}_3(21\bar{3}1)$ has one of the largest enantioselective potentials due to inhomogeneity of atoms on the surface, where both Ca and O atoms are present (figure 1). Interestingly, the major quartz faces do not show very large chiral indices. This result is surprising since the bulk structure of quartz is chiral, but when the surfaces are examined the arrangement of the exposed O atoms are close to a mirror symmetry [27]. Recently, Kahr and co-workers examined the adsorption of carminic acid on quartz($10\bar{1}0$) surface using interatomic potentials and found that the quartz surface does not provide an enantiospecific surface [28].

In this paper we report the first theoretical study of amino acid adsorption on the chiral calcite($21\bar{3}1$) surface. In particular, we determine the relevant local minima of both enantiomers of Ala on the $\text{CaCO}_3(21\bar{3}1)$ surface to determine the degree of enantiospecificity. The aqueous system of the experiments is difficult to simulate directly using first-principles due to the computational cost and lack of knowledge of the details of the adsorbate/calcite interface. As a first step we only examine the amino acid-mineral surface and neglect the role of the solvent. To make contact between our DFT studies and the experiments requires several assumptions. We assume that there is a direct and strong interaction between the amino acid and the mineral surface. This assumption is based on the strong adsorption observed for amino acids on calcite($21\bar{3}1$) observed by Hazen and co-workers. Simple washing with water did not remove the bound amino acids, and an acid etch was needed to remove the amino acid from the surface. Even with a direct amino acid-mineral interface the solvent can be expected to change the strength of binding due to stabilization of the surface and/or the adsorbate and furthermore both the adsorbate and surface will be sensitive to the pH of the solvent. Nevertheless, if we assume that the solvent effect is equal for both enantiomers we would expect that the differences between the adsorption energies of the two enantiomers will still be dictated by differences in the interactions at the molecule-mineral interface. Since we are interested in the enantiospecific binding of the amino acid on the surface, the reference state of the molecule in the aqueous solution and transport of the molecule to the surface is not needed. Based on the above arguments we

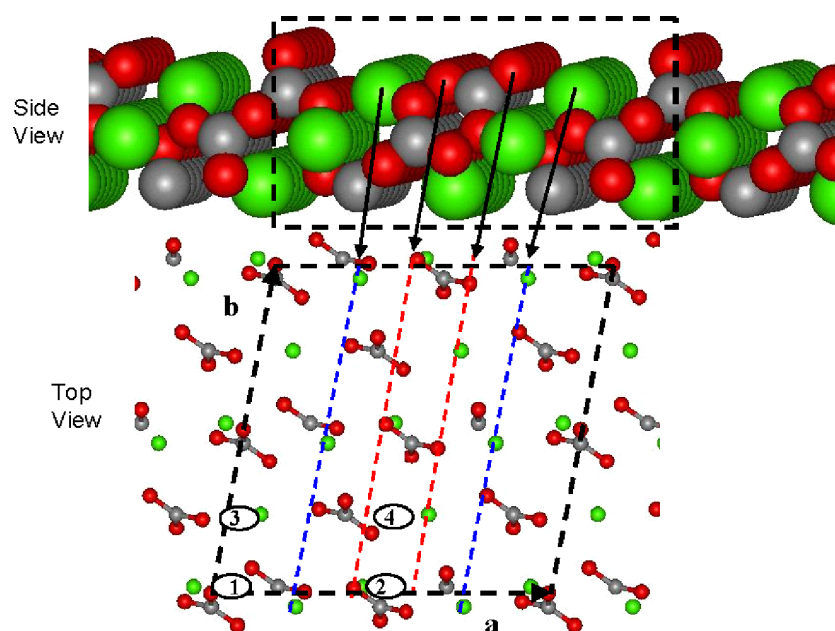


Figure 1. A side and top view of the calcite(21̄31) surface. The black dashed lines indicate the unit cell used in our calculations and the colored dashed lines and arrows are to assist the reader in seeing the surface atoms in the top view. The numbered dark ellipses represent the initial sites for the alanine molecule. Note the ellipses roughly represent the location of the chiral carbon atom over the calcite surface, but not the size of the Ala molecule. The unit cell dimensions are $12.85 \times 12.75 \text{ \AA}$ (colour in online version).

expect that the enantiospecific binding energies reported in this paper (see equation (2) below) will qualitatively follow the trends expected in the solvent system and would serve as an upper bound on the enantiospecific binding.

There are other modeling approaches available to examine this system. Earlier modeling studies of Asp adsorption on the steps and flat surface of calcite(10̄11) used semi-empirical methods [26]. They examined different minima for both enantiomers on various sites on the step edge and surface. Water was modeled as a continuum dielectric, which screens the interactions between adsorbate and surface, and hydrophobic interactions are approximated in the semi-empirical potential. While semi-empirical methods can incorporate water at some level, the drawbacks are that the system interactions are normally fitted to solvation data and might not necessarily capture the amino acid–mineral interactions accurately. Furthermore the semi-empirical study did not incorporate mineral surface relaxation in response to the interaction with the amino acid. This relaxation could be especially important if the molecule modifies the surface structure, as would be expected for strongly interacting systems. Another approach would be to use molecular dynamics based on classical potentials. Accurate potentials would have to be developed that describe all the different interactions in the system, including water–adsorbate and water–mineral surface interactions. This approach has been used to examine water on the calcite(10̄11) surface successfully [29]. The DFT results presented in this paper can be a first step in generating amino acid–calcite data needed to fit classical potentials for this system.

2. Simulation methods & details

All DFT calculations in this paper were performed using VASP (Vienna *ab initio* simulation package) [30–33] with the ion cores represented by ultrasoft pseudopotentials found in the database provided by VASP [34–37]. Calculations were done with the generalized gradient approximation (GGA), using the Perdew–Wang 91 functional [38,39]. DFT–GGA calculations have been shown to give accurate results for amino acid adsorption on various metal surfaces [16,19,20,40]. A plane wave expansion with a cutoff of 400 eV was used. The positions of the atoms were relaxed using the Newton–Raphson or CG method until the forces on all unconstrained atoms were less than 0.05 eV/\AA . The calcite(21̄31) surface is allowed to relax along with the Ala adsorbate. We found that fixing the mineral surface atoms results in an order of magnitude weaker binding of the adsorbate. Due to the size of the system, we performed all calculations using just the Γ point. All calculations were done with the experimental lattice parameter of calcite ($a = 4.990 \text{ \AA}$).

The first task, to define the relaxed calcite(21̄31) surface, is non-trivial. The atomic geometry of the truncated calcite(21̄31) surface is not uniquely defined, since parallel planes will have different atoms exposed on the surface. Furthermore, simply using the (21̄31) plane as a cleaving plane will result in surfaces that expose oxygen atoms that do not belong to a CO_3 group. Therefore, we have defined our surface by truncating the (21̄31) plane at the Ca–C atom layer and then removing the Ca and C atoms on the top layer along with the O atoms bonded to the surface C atom. Any O atom that remains on the surface that is not part of a CO_3 group is also removed.

The net result of this procedure is that all O atoms on the surface are part of complete CO_3 group. Side and top views of the calcite(21 $\bar{3}$ 1) surface used in all of our calculations is shown in figure 1. We have found that this is the only surface that is stable in our DFT calculations. In our calculations of the amino acid on the surface we only use the calcite(21 $\bar{3}$ 1) surface shown in figure 1 and examine adsorption of the two enantiomers of the amino acid. This set of calculations will give exactly the same result as the adsorption of one enantiomer on the calcite(21 $\bar{3}$ 1) and its mirror (3 $\bar{1}$ 21) surface.

As noted in the introduction, we do not model directly the effects of water on the calcite surface. There has been considerable theoretical [29,41] and experimental [42,43] work on determining the exact nature of the water–calcite interface, but this work has concentrated on the dominant achiral calcite(10 $\bar{1}$ 1) surface. Recent surface X-ray scattering study by Goldschmidt *et al.* derived detailed information on the water–calcite(10 $\bar{1}$ 1) interface and they find an ideal termination (i.e. no reconstruction) with a ordered monolayer of water composed of two distinct water molecules per unit cell [42,43]. To our knowledge there have not been similar studies of the calcite(21 $\bar{3}$ 1) surface, but in the absence of such knowledge we assume no reconstruction. We have assumed that the adsorbate interacts with the calcite(21 $\bar{3}$ 1) surface directly (see Section 1), therefore we model the surface as terminated by O and Ca atoms and not hydroxyl or water molecules.

Our supercell consists of a (2 × 1) calcite(21 $\bar{3}$ 1) with a slab thickness of 3 CaCO_3 units and with the bottom CaCO_3 unit fixed in its bulk position. This procedure results in a slab with dimensions 12.8 × 12.8 Å and a thickness of 3 Å. The lateral dimensions are large enough to minimize molecule–molecule interactions. A minimum vacuum spacing of 15 Å was used in all of our calculations to minimize spurious interactions in the direction normal to the surface. We relaxed the bare calcite(21 $\bar{3}$ 1) surface and found a relatively small degree of relaxation on the surface. The exposed surface Ca atoms relax into the surface to more strongly bind to the O atoms. One of the CO_3 groups also relaxes inward but overall the CO_3 groups maintain their bulk alignment. Due to computational expense of these DFT calculations, we have had to use a relatively thin slab. We have confirmed that this thickness does not qualitatively affect the results discussed in this paper by performing calculations of the bare surface and D-Ala adsorption of one specific configuration on slabs with 4 CaCO_3 units. The bare surface relaxation is not substantially different in thicker slabs. For instance, the two $\text{Ca}_{\text{surf}}\text{--O}$ distances are 2.175 (2.179) and 2.324 (2.336) Å for the thinner (thicker) slab. The adsorption energy for D-Ala on the test configuration was within the estimated error of our DFT calculations.

We have examined the adsorption of Ala with the carboxyl group protonated. The actual configuration at a solvent–surface interface will depend on the pH and we will study the affects of protonation and deprotonation of the amino and carboxyl group in the future. The relaxed

structure of L-Ala obtained from our DFT calculations is very similar to that determined for glycine by Rankin and Sholl [20].

To determine the enantiospecificity of Ala on the calcite(21 $\bar{3}$ 1) surface we need to find the relevant local minima for both enantiomers on the surface. Since we do not have any information from experiment to assist us in defining plausible binding geometries and sites we have had to perform a more systematic search. We have defined two orientations for the Ala molecule with respect to the surface. The first orientation type (referred to as O^{up}) has the H group from the chiral center carbon and the carboxyl group pointed towards the calcite surface and the amino and methyl groups pointed away from the surface. The second orientation type (O^{down}) has the methyl and amino group pointed towards the surface along with the carboxyl group. The two orientation classes are related by a rotation in the YZ plane (or a flip operation). The two orientations will bring different functional groups to interact with the surface.

We choose an initial site, marked 1 on figure 1, and place the carbon atom that is the chiral center in Ala above the surface O atom. The chiral carbon–carboxyl group bond is parallel to the *a*-direction (see figure 1 for the definition of the *a* and *b* surface lattice vectors). We then generated other configurations by performing translations and rotations around the surface normal for both orientations. We performed three translations from site 1: the first is a 1/4 unit cell translation in the *b*-direction (labeled site 2), the second is a 1/2 unit cell translation in the *a*-direction (labeled site 3), and finally translations in both *a*- and *b*-directions (labeled site 4). We also performed a 180° rotation of the molecule at each of the sites. We will refer to the different configurations as follows. O_i^{up} refers to a configuration with Ala in the up orientation located at site *i*, while RO_i^{up} the same configuration but with the rotation operation. Similar configurations are generated using the down configuration and denoted O_i^{down} and $\text{RO}_i^{\text{down}}$.

The above procedure yields 16 unique configurations for a single enantiomer of Ala. The relaxation to a local minimum can be computationally time consuming due to a wide range of intramolecular, intracrystalline, and crystal–molecule interactions in this system. We have also tested the effect of small displacements in the initial configurations and found that it greatly reduces the computational cost of the calculations if the configuration is moved to allow an initial $\text{Ca}_{\text{surf}}\text{--O}_{\text{Ala}}$ distance of 2.3 Å, which is approximately that found in bulk calcite and other minerals with Ca–O bonds [44]. Some of the initial configurations are not at stable sites (this occurs mainly if the oxygen atoms from the molecule are brought into close proximity with oxygen atoms on the surface) and we terminate a minimization if the surface is greatly distorted. It is impossible to absolutely rule out that a relevant minimum is not identified by our search, but our procedure brings all the different combinations of atoms on the molecule to the surface atoms.

The various initial configurations are relaxed to obtain a range of local minima. The binding energy for the D enantiomer, U_i^D , can be defined by

$$U_i^D = (E_{\text{Ala}} + E_{\text{slab}}) - E_{\text{Ala-slab},i} \quad (1)$$

where E_{Ala} is the energy of the isolated Ala molecule (both enantiomers have the same energy), E_{slab} is the energy of the relaxed $\text{CaCO}_3(21\bar{3}1)$ slab, and $E_{\text{Ala-slab},i}$ is the energy of the local minima, i , for the amino acid on the calcite surface. A similar equation holds for the L enantiomer (U_i^L). We stress that the binding energy should not be taken as an observable adsorption energy in either gas-phase or solvent experiments. The exact Ala structure that would be adsorbed in a gas-phase experiment is not known and, for experiments involving a solution, the isolated Ala is not the proper reference energy. Nevertheless, the adsorption energy does give the relative importance of different minima to the adsorption behaviour of the amino acid on the surface. The parameter we are more interested in, and which can be defined uniquely, is the difference in binding energy of the global minimum between the two enantiomers, i.e. the enantiospecific binding energy (ΔU_o), defined by

$$\Delta U_o = U_o^D - U_o^L = E_{\text{Ala-slab},o}^D - E_{\text{Ala-slab},o}^L \quad (2)$$

where the o subscript indicates the global (or the most stable) minima that we find for each enantiomer. If ΔU_o is positive then the L-Ala will be preferentially bound on the calcite(2131) surface. While we have estimated errors of 2.3 kcal/mol (0.1 eV) in the total energies found in equations (1) and (2), we can discuss enantiospecific binding energies that are much smaller (~ 0.5 kcal/mol) since there is a cancellation of systematic errors in applying equation (2) [16].

3. Results and discussion

The different initial configurations described in section 2 were minimized to find local minima for D-Ala. Table 1 shows the energies for the stable minima for D-Ala that we were able to identify in our search. A few of the sites resulted in major distortion of the CO_3 groups on the surface and did not minimize to a stable site (labeled

Table 1. Identified adsorption minima (kcal/mol) from different starting configurations for D-alanine on the calcite(2131) surface. See text for explanation of the configuration notation.

Configuration	Orientation up	Orientation down
O ₁	42.1	48.0
O ₂	32.50	23.3
O ₃	Unstable	25.5
O ₄	Unstable	19.8
RO ₁	19.5	16.6
RO ₂	8.1	Unstable
RO ₃	24.8	22.5
RO ₄	Unstable	Unstable

unstable in table 1). For both orientations we find that the O₁ site is the most stable. For the up orientation the O₁ site is 10 kcal/mol more stable than the second most stable minima at the O₂ site and for the down orientation the O₁ site is at least 13 kcal/mol more stable than any other site. We have applied several mirror operations on the two stable configurations (O₁^{up} and O₁^{down}) of D-Ala to generate L-Ala configurations, which are then minimized. This procedure allows us to examine the most likely stable sites for L-Ala without having to perform the exhaustive search that we have done for D-Ala. We have confirmed with a few test calculations that the other sites do not produce more stable sites for L-Ala. Below we discuss the energetics and geometry of D- and L-Ala adsorbed on the O₁^{up} and O₁^{down} sites.

For the O₁^{up} site we find a stable minimum for L-Ala of 43.6 kcal/mol. This results in an enantiospecific binding energy, ΔU_o , of -0.8 kcal/mol for Ala in the up orientation. For the O₁^{down} site we find a stable minimum for L-Ala of 47.2 kcal/mol, which gives an enantiospecific binding energy, ΔU_o , of $+0.8$ kcal/mol for Ala in the down orientation. Both these values for enantiospecific binding are substantially smaller than observed by Sljivancanin *et al.* [16] and Bhatia and Sholl [17] for chemisorption on chiral metal surfaces, and are on the order of the observed values for physisorption on chiral metal surfaces.

Figure 2(a),(b) shows the side and top view of the most stable configuration (O₁^{up}) for both enantiomers of Ala in the up orientation. The parameters describing the structure of D- and L-Ala adsorbed on this site along with the same values for isolated Ala are shown in table 2. Some relevant bond distances between the amino acid and the calcite surface are also included in table 2. Examining figure 2(a), we observe very little difference of the calcite(2131) surface between the two enantiomers. In particular the calcite surface appears to undergo the same type of relaxation with both enantiomers of Ala. This result implies that the surface “sees” no difference between the two enantiomers of Ala—a result that can be confirmed by examining the structure of the amino acid upon adsorption. From table 2 we observe that the bond distances of D- and L-Ala show negligible differences. The main difference between the bond distances found in free and bound Ala is in the carboxyl group. Upon adsorption the C=O bond is very slightly weakened (C=O distance increases from 1.22 to 1.24 Å) and the C—OH bond is strengthened (C—OH distance decreases from 1.35 to 1.31 Å) for both enantiomers. The change in the carboxyl group is due to the new interaction between the O atom of the amino acid with Ca atom on the surface. The bond angles show more variability than the bond distances, which indicates that there is some distortion of the molecule due to the interactions with the surface. Figure 2(b) shows the top view of the same minima as in figure 2(a). The dashed line in figure 2(b) represents the approximate mirror relating the two enantiomers of Ala. Table 2 shows that the Ca—O_{Ala} and distance and orientation are very similar in both

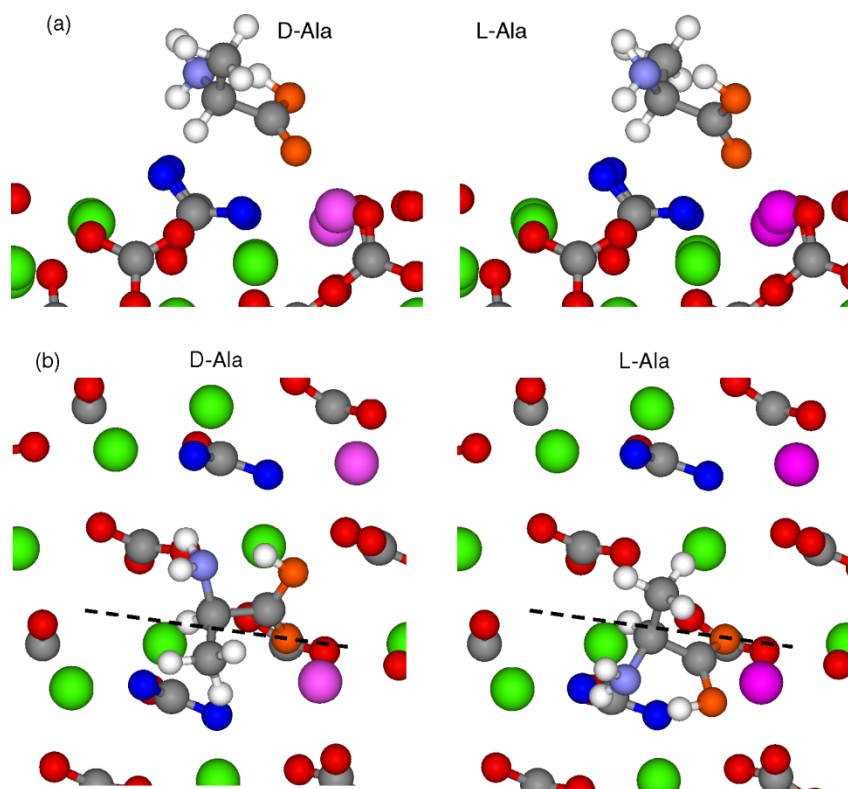


Figure 2. (a) Side and (b) top view of the most stable local minimum (O_1^{up}) found for both enantiomers of Ala in the up orientation on calcite(21 $\bar{3}$ 1). The atom color is coordinated between the top and side views. The dashed line in the top view represents the mirror plane relating the two enantiomers (colour in online version).

enantiomers. The distance between an H atom of the chiral C and a surface O atom ($O_{\text{surf}}\text{---}H_{\text{AA}}(\text{C}^*)$) is different for the two enantiomers, but this difference has little effect on the energy since the distance is over 2 Å for both enantiomers. The methyl and amino group are obviously at different locations for the two enantiomers and the L-enantiomer brings a H on the NH_2 group close to a surface O atom

Table 2. Structural details for D- and L-alanine adsorbed on the O_1^{up} site. D-Ala is favored by 0.8 kcal/mol for this site. Structural parameters for isolated Ala are provided for reference. Bond distances greater than 2.5 Å are not shown.

	D-Ala (O_1^{up})	L-Ala (O_1^{up})	Ala (isolated)
Bond distances (Å)			
C=O	1.24	1.25	1.22
C—OH	1.31	1.31	1.34
O—H	1.04	1.05	1.01
C—C	1.53	1.53	1.54
C1—H	1.10	1.10	1.10
N—H	1.02	1.02	1.02
C—N	1.47	1.47	1.47
Bond angles (degrees)			
O=C—O	122.7	122.1	123.8
C—C=O	124.1	124.4	123.0
C—C—OH	113.2	113.4	113.2
C—C—C	110.0	111.2	109.8
C—C—N	105.7	104.8	109.5
Distances (Å) between amino acid and calcite surface			
$O_{\text{AA}}\text{---}Ca$	2.17	2.17	—
$(\text{C}^*)H_{\text{AA}}\text{---}O_{\text{surf}}$	2.34	2.46	—
$(\text{N})H_{\text{AA}}\text{---}O_{\text{surf}}$	—	2.10	—

($O_{\text{surf}}\text{---}H_{\text{AA}}(\text{NH}_2)$ in table 2 is 2.10 Å). The interaction of the methyl and amino groups with the surface is weak due to the relatively long distance, as can be seen by examining figure 2(a) and by the negligible change in bond lengths associated with these groups. The above observations match with the small energy differences observed between the two enantiomers adsorbed in the O_1^{up} site. The main point of interaction for both enantiomers is between the surface Ca atom and the O atom from the carboxyl group.

Figure 3(a),(b) and table 3 provide the same information as figure 2(a),(b) and table 2 but for Ala in the configuration O_1^{down} , where the methyl and amino groups are pointing towards the surface. Examining figure 3(a), we observe that the calcite surface shows slightly different relaxation, dependent on the adsorbed enantiomer. In particular, the top most row of Ca atoms shows more rumpling when the L-enantiomer is adsorbed. The rotation of the CO_3 group directly under the Ala molecule is very similar for both enantiomers. The top view shown in figure 3(b) illustrates some of the differences between the two enantiomers adsorbed on this site. On the one hand, for the D-enantiomer the protonated O atom interacts with the Ca atom and the amino group is near the surface O atom, while for the L-enantiomer the Ca atom interacts with the non-protonated O atom and the methyl group is near the surface O atom. These differences between the two enantiomers are not sufficient to induce a large difference in adsorption energy, because the dominant interaction is still between the Ca surface atom and the O atom of the carboxyl group on Ala.

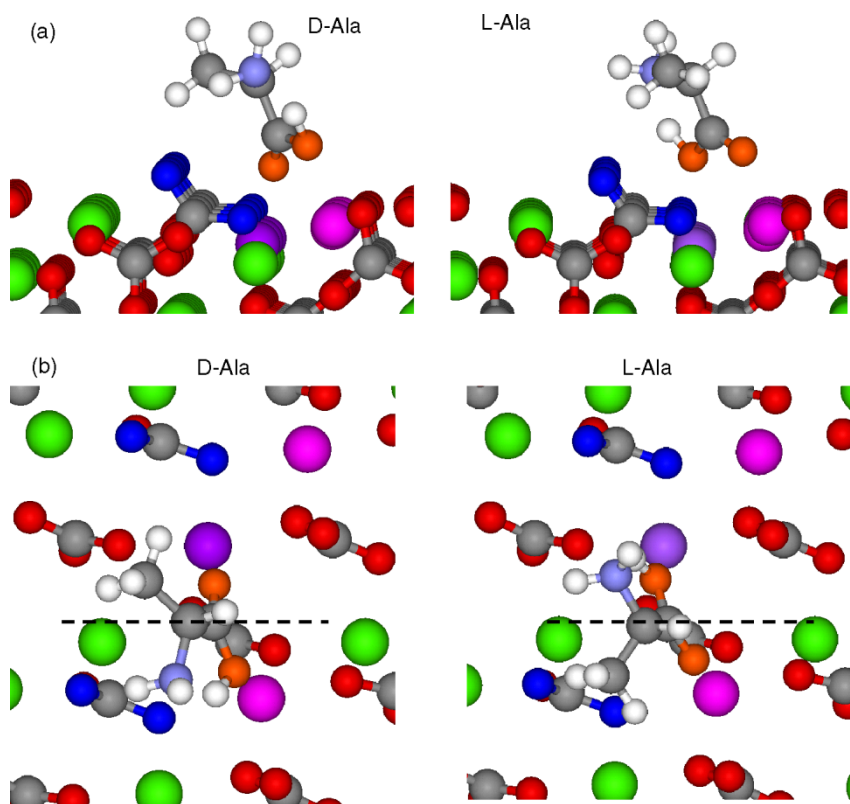


Figure 3. (a) Side and (b) top view of the most stable local minimum (O_1^{down}) found for both enantiomers of Ala in the down orientation on calcite(2131). The atom color is coordinated between the top and side views. The dashed line in the top view represents the mirror plane relating the two enantiomers.

Examining the structural data in table 3, we observe again that the bond distances of the two enantiomers are similar. Furthermore both enantiomers have bond distances very similar to the unbound Ala molecule, but again the bond angles are different indicating that the molecule is slightly distorted due to the surface interaction, but does not lose much strength in the

intramolecular bonds. The $\text{Ca}-\text{O}_{\text{AA}}$ distance is slightly larger for the D-enantiomer than the L-enantiomer (2.18 versus 2.12 Å), indicating a slightly weaker $\text{Ca}-\text{O}_{\text{AA}}$ bond for the D-enantiomer. These observations indicate that the L-enantiomer interactions with the surface are slightly weaker than the D-enantiomer, leading to a small enantiospecific affect favoring L-Ala for this configuration. The interaction between the O surface groups and amino versus methyl group is weak and not sufficiently different to produce a larger enantiospecific affect. Once again the observations for the O_1^{down} configuration reinforce the dominant role of the $\text{Ca}-\text{O}$ interactions in this system (figure 3).

Why does Ala show such poor enantiospecific behavior on calcite(2131), especially when there are obvious strong interactions between the molecule and the surface? As noted by others [5,16] three points of interaction are needed to show strong enantiospecificity. This condition is not met in the Ala/calcite(2131) system, mainly because the Ala molecule is not large enough to form strong interactions with three points of the calcite surface. In particular on the calcite(2131) surface, the O surface atoms in the *b*-direction are separated by about 6 Å and the same is true for the Ca atoms. The size of the Ala molecule is approximately 3–4 Å depending on the dimension chosen; therefore the molecule cannot span the Ca–Ca (or $\text{O}_{\text{surf}}-\text{O}_{\text{surf}}$) distances. This size disparity is illustrated in figure 4, where we show the Ala molecule on the surface with a triangle to highlight three points on the calcite

Table 3. Structural details for D- and L-Ala adsorbed on the O_1^{down} site. L-Ala is favored by 0.8 kcal/mol for this site. Structural parameters for isolated Ala are provided for reference. Bond distances greater than 2.5 Å are not shown.

	D-Ala (O_1^{down})	L-Ala (O_1^{down})	Ala (isolated)
Bond distances (Å)			
C=O	1.23	1.23	1.22
C–OH	1.34	1.34	1.34
O–H	1.08	1.04	1.01
C–C	1.53	1.53	1.54
C–H	1.10	1.10	1.10
N–H	1.02	1.02	1.02
C–N	1.49	1.47	1.47
Bond angles (degrees)			
O=C–O	122.0	122.1	123.8
C–C=O	128.3	123.9	123.0
C–C–OH	109.7	114.0	113.2
C–C–C	115.7	111.8	109.8
C–C–N	103.2	106.5	109.5
Distances (Å) between amino acid and calcite surface			
$\text{O}_{\text{AA}}-\text{Ca}$	2.18	2.12	–
$(\text{NH}_2)\text{H}_{\text{AA}}-\text{O}_{\text{surf}}$	–	–	–
$(\text{CH}_3)\text{H}_{\text{AA}}-\text{O}_{\text{surf}}$	–	2.40	–

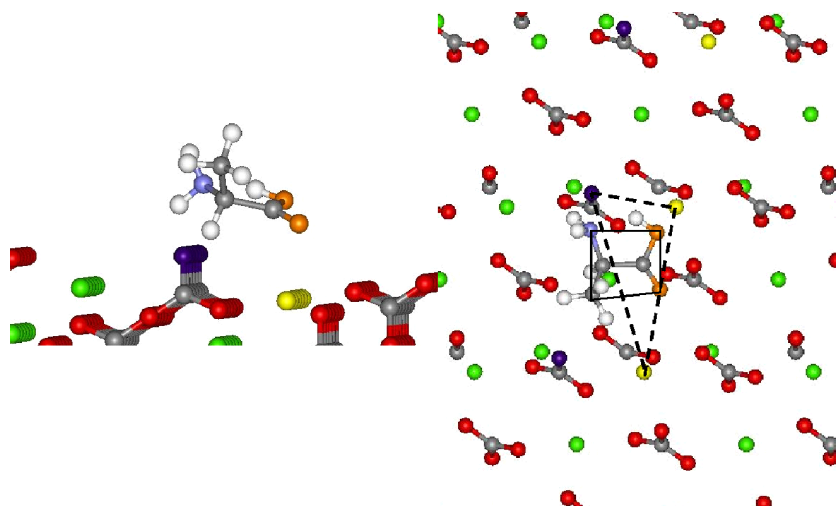


Figure 4. Ala molecule on calcite(21 $\bar{3}$ 1). The surface O and Ca atoms are represented by purple and yellow atoms. The dashed triangle is created from three surface atoms that can interact with an adsorbate and the box shows the effective size of the Ala molecule (colour in online version).

surface. The carboxyl group on Ala can interact with only one of the Ca atoms on the surface, and only one of the other groups can interact with the O atom on the surface. Because of this disparity in the two systems, strong three-point interactions are not possible. This result implies that pH should not greatly effect the enantiospecific behavior of the Ala molecule on calcite(21 $\bar{3}$ 1). The main role of pH will be to modify the functional groups on Ala by protonation and deprotonation therefore modifying the strength of particular mineral–molecule intermolecular interactions, but will not introduce any new interactions to induce a three-point complex.

Experimental work by Hazen *et al.* have shown negligible enantiospecificity for Ala on calcite(21 $\bar{3}$ 1) [45], which matches the prediction from our modeling. Our analysis indicates that larger amino acids that can potentially bridge the surface O and Ca atoms might show stronger enantiospecificity. Furthermore, Ala on calcite(21 $\bar{3}$ 1) may still show enantiospecific adsorption if there are dominant interactions with steps or other defects on the surface. As shown by Orme *et al.*, Asp has chiral interactions on the achiral calcite(10 $\bar{1}$ 1) surface due to the presence of steps [26]. Teng *et al.* see strong enantiospecific effects when calcite(10 $\bar{1}$ 1) is grown in the presence of enantiopure Ala [46]. The results of Teng *et al.* indicate that the steps on calcite(10 $\bar{1}$ 1) provide an enantiospecific environment for Ala, likely due to the more restricted geometry for the amino acid adsorbed on step edges. Further studies of adsorption of Ala on growth steps of calcite(21 $\bar{3}$ 1) will be needed to determine the role of steps on the enantiospecific behavior of this system.

4. Conclusions

We have examined the adsorption of both enantiomers of Ala on the chiral calcite(21 $\bar{3}$ 1) surface using DFT. We find negligible differences in binding energy and structure for

the global minimum of the D- and L-Ala on the calcite(21 $\bar{3}$ 1) surface. Other minima identified show relatively weak enantiospecificity, as well. The source of the weak enantiospecificity for this system is the size disparity between the Ala molecule and the distances between surface atoms on the calcite(21 $\bar{3}$ 1) surface. The small Ala molecule cannot interact strongly with three points on the surface, resulting in the weak enantiospecificity observed. Our results indicate that larger amino acids, such as Asp, may show stronger enantiospecificity, and we are currently examining the adsorption of Asp on calcite(21 $\bar{3}$ 1) to confirm this hypothesis. The prediction based on our calculations of weak enantiospecificity for Ala on calcite(21 $\bar{3}$ 1) is in qualitative agreement with the experimental results of Hazen *et al.* [45]. This initial study shows the promise of combining DFT calculations with experimental work to enhance our understanding of amino acid–mineral interactions.

Acknowledgements

We thank Henry Teng, Andrew Gellman, David Sholl, and Robert Downs for helpful discussions. This work was supported by NSF (EAR0229634), the NASA Astrobiology Institute, and the Carnegie Institution of Washington.

References

- [1] R.M. Hazen. Life's rocky start. *Sci. Am.*, **284**, 76 (2001).
- [2] R.M. Hazen, T.R. Filley, G.A. Goodfriend. Selective adsorption of L- and D-amino acids on calcite: implications for biochemical homochirality. *Proc. Natl Acad. Sci. USA*, **98**, 5487 (2001).
- [3] N. Lahav. *Biogenesis: Theories of Life's Origin*, Oxford University Press, New York, NY (1999).
- [4] R.M. Hazen. Chiral crystal faces of common rock-forming minerals. In *Progress in Biological Chirality*, G. Palyi, C. Zucchi, L. Caglioti (Eds.), p. 137, Elsevier, Oxford (2004).
- [5] R.M. Hazen, D.S. Sholl. Chiral selection on inorganic crystalline surfaces. *Nat. Mater.*, **2**, 367 (2003).

- [6] D.S. Sholl, A. Asthagiri, T.D. Power. Naturally chiral metal surfaces as enantiospecific adsorbents. *J. Phys. Chem. B*, **105**, 4771 (2001).
- [7] A.J. Gellman, J.D. Horvath, M.T. Buelow. Chiral single crystal surface chemistry. *J. Mol. Catal. A-Chem.*, **167**, 3 (2001).
- [8] T.D. Power, D.S. Sholl. Effects of surface relaxation on enantiospecific adsorption on naturally chiral Pt surfaces. *Topics Catal.*, **18**, 201 (2002).
- [9] T.D. Power, A. Asthagiri, D.S. Sholl. Atomically detailed models of the effect of thermal roughening on the enantiospecificity of naturally chiral platinum surfaces. *Langmuir*, **18**, 3737 (2002).
- [10] T.D. Power, D.S. Sholl. Enantiospecific adsorption of chiral hydrocarbons on naturally chiral Pt and Cu surfaces. *J. Vac. Sci. Tech. A*, **17**, 1700 (1999).
- [11] A. Asthagiri, P.J. Feibelman, D.S. Sholl. Thermal fluctuations in the structure of naturally chiral Pt surfaces. *Topics Catal.*, **18**, 193 (2002).
- [12] J.D. Horvath, A.J. Gellman, D.S. Sholl, T.D. Power. Enantiospecific properties of chiral single crystal surfaces. *Phys. Chem. Chirality*, (2000), American Chemical Society.
- [13] J.D. Horvath, A. Koritnik, P. Kamakoti, D.S. Sholl, A.J. Gellman. Enantioselective separation on naturally chiral surfaces. *J. Am. Chem. Soc.*, **126**, 14988 (2004).
- [14] J.D. Horvath, A.J. Gellman. Enantiospecific desorption of R- and S-propylene oxide from a chiral Cu(643) surface. *J. Am. Chem. Soc.*, **123**, 7953 (2001).
- [15] D.S. Sholl. Adsorption of chiral hydrocarbons on chiral platinum surfaces. *Langmuir*, **14**, 862 (1998).
- [16] Z. Slijivancanin, K.V. Gothelf, B. Hammer. Density functional theory study of enantiospecific adsorption at chiral surfaces. *J. Am. Chem. Soc.*, **124** (2002).
- [17] B. Bhatia, D.S. Sholl. Enantiospecific chemisorption of small molecules on intrinsically chiral Cu surfaces. *Angew. Chem. Int. Ed.*, **44**, 7761 (2005).
- [18] S.M. Barlow, R. Raval. Complex organic molecules at metal surfaces: bonding, organisation and chirality. *Surf. Sci. Rep.*, **50**, 201 (2003).
- [19] R.B. Rankin, D.S. Sholl. Structure of enantiopure and racemic alanine adlayers on Cu(110). *Surf. Sci.*, **574**, L1 (2005).
- [20] R.B. Rankin, D.S. Sholl. Assessment of heterochiral and homochiral glycine adlayers on Cu(110) using density functional theory. *Surf. Sci.*, **548**, 301 (2004).
- [21] A. Asthagiri, D.S. Sholl. Pt thin films on stepped SrTiO₃ surfaces: SrTiO₃(620) and SrTiO₃(622). *J. Mol. Catal. A*, **216**, 233 (2004).
- [22] K. Soai, S. Osanai, K. Kadowaki, S. Yonekubo, T. Shibata, I. Sato. D- and L-quartz-promoted highly enantioselective synthesis of a chiral organic compound. *J. Am. Chem. Soc.*, **121**, 11235 (1999).
- [23] I. Sato, K. Kadowaki, K. Soai. Asymmetric synthesis of an organic compound with high enantiomeric excess induced by inorganic ionic sodium chlorate. *Angew. Chem. Int. Ed.*, **39**, 1510 (2000).
- [24] H.H. Teng, P.M. Dove. Surface site-specific interactions of aspartate with calcite during dissolution: implications for biomineralization. *Am. Mineralogist*, **82**, 878 (1997).
- [25] H.H. Teng, P.M. Dove, C.A. Orme, J.J. De Yoreo. Thermodynamics of calcite growth: baseline for understanding biomineral formation. *Science*, **282**, 724 (1998).
- [26] C.A. Orme, A. Noy, A. Wierzbicki, M.T. McBride, M. Grantham, H.H. Teng, P.M. Dove, J.J. DeYoreo. Formation of chiral morphologies through selective binding of amino acids to calcite surface steps. *Nature*, **411**, 775 (2001).
- [27] R.T. Downs, R.M. Hazen. Chiral indices of crystalline surfaces as a measure of enantioselective potential. *J. Mol. Catal. A-Chem.*, **216**, 273 (2004).
- [28] B. Kahr, B. Chittenden, A. Rohl. Robert Boyle's chiral crystal chemistry: computational re-evaluation of enantioselective adsorption on quartz. *Chirality*, **18**, 127 (2006).
- [29] S. Kerisit, S.C. Parker, J.H. Harding. Atomistic simulation of the dissociative adsorption of water on calcite surfaces. *J. Phys. Chem. B*, **107**, 7676 (2003).
- [30] G. Kresse, J. Furthmuller. Efficiency of *ab-initio* total energy calculations for metals and semiconductors using a plane-wave basis set. *Comp. Mater. Sci.*, **6**, 15 (1996).
- [31] G. Kresse, J. Furthmuller. Efficient iterative schemes for *ab initio* total-energy calculations using a plane-wave basis set. *Phys. Rev. B*, **54**, 11169 (1996).
- [32] G. Kresse, J. Hafner. *Ab-initio* molecular-dynamics simulation of the liquid-metal amorphous-semiconductor transition in germanium. *Phys. Rev. B*, **49**, 14251 (1994).
- [33] G. Kresse, J. Hafner. *Ab-initio* molecular-dynamics for liquid-metals. *Phys. Rev. B*, **47**, 558 (1993).
- [34] A. Pasquarello, K. Laasonen, R. Car, C.Y. Lee, D. Vanderbilt. *Ab initio* molecular-dynamics for d-electron systems—liquid copper at 1500-K. *Phys. Rev. Lett.*, **69**, 1982 (1992).
- [35] K. Laasonen, A. Pasquarello, R. Car, C.Y. Lee, D. Vanderbilt. Car-Parrinello molecular dynamics with Vanderbilt ultrasoft pseudopotentials. *Phys. Rev. B*, **55**, 13953 (1993).
- [36] D. Vanderbilt. Soft self-consistent pseudopotentials in a generalized eigenvalue formalism. *Phys. Rev. B*, **41**, 7892 (1990).
- [37] G. Kresse, J. Hafner. Norm-conserving and ultrasoft pseudopotentials for first-row and transition-elements. *J. Phys. Condens. Matter*, **6**, 8245 (1994).
- [38] J.P. Perdew, Y. Wang, unpublished.
- [39] J.P. Perdew. *Electronic Structure of Solids '91*, P. Eschrig (Ed.), Akademie Verlag, Berlin (1991).
- [40] L.A. Barbosa, P. Sautet. Stability of chiral domains produced by adsorption of tartaric acid isomers on the Cu(110) surface: a periodic density functional theory study. *J. Am. Chem. Soc.*, **123**, 6639 (2001).
- [41] K. Wright, R.T. Cygan, B. Slater. Structure of the (10(1)over-bar4) surfaces of calcite, dolomite and magnesite under wet and dry conditions. *Phys. Chem. Chem. Phys.*, **3**, 839 (2001).
- [42] P. Geissbuhler, P. Fenter, E. DiMasi, G. Srajer, L.B. Sorensen, N.C. Sturchio. Three-dimensional structure of the calcite-water interface by surface X-ray scattering. *Surf. Sci.*, **573**, 191 (2004).
- [43] P. Fenter, P. Geissbuhler, E. DiMasi, G. Srajer, L.B. Sorensen, N.C. Sturchio. Surface speciation of calcite observed *in situ* by high-resolution X-ray reflectivity. *Geochim. Cosmochim. Acta*, **64**, 1221 (2000).
- [44] J.R. Smyth, D.L. Bish. *Crystal Structures and Cation Sites of the Rock-Forming Minerals*, Allen & Unwin, Boston (1988).
- [45] R.M. Hazen, J.A. Brandes, H.S.J. Yoder. Possible roles of minerals in the prebiotic synthesis and selection of amino acids. *Trans. Am. Geophys. Union* (Abstract) (2002).
- [46] H.H. Teng, unpublished.